Plasma Sci. Technol. **20** (2018) 065402 (8pp) https://doi.org/10.1088/2058-6272/aaac79

Plasma characteristics of direct current enhanced cylindrical inductively coupled plasma source

Yue HUA (滑跃), Jian SONG (宋健), Zeyu HAO (郝泽宇) and Chunsheng REN (任春生)

Key Laboratory of Materials Modification by Laser, Ion and Electron Beams, Dalian University of Technology, Ministry of Education, Dalian 116024, People's Republic of China

E-mail: rchsh@dlut.edu.cn

Received 26 November 2017, revised 30 January 2018
Accepted for publication 31 January 2018
Published 2 May 2018

Abstract

Experimental results of a direct current enhanced inductively coupled plasma (DCE-ICP) source which consists of a typical cylindrical ICP source and a plate-to-grid DC electrode are reported. With the use of this new source, the plasma characteristic parameters, namely, electron density, electron temperature and plasma uniformity, are measured by Langmuir floating double probe. It is found that DC discharge enhances the electron density and decreases the electron temperature, dramatically. Moreover, the plasma uniformity is obviously improved with the operation of DC and radio frequency (RF) hybrid discharge. Furthermore, the nonlinear enhancement effect of electron density with DC + RF hybrid discharge is confirmed. The presented observation indicates that the DCE-ICP source provides an effective method to obtain high-density uniform plasma, which is desirable for practical industrial applications.

Keywords: cylindrical ICP, DC + RF hybrid discharge, nonlinear enhancement effect

(Some figures may appear in colour only in the online journal)

1. Introduction

With the rapid development of semiconductor manufacturing, various plasma sources based on different mechanisms of electromagnetic power absorption, e.g., inductively coupled plasma (ICP) sources, capacitively coupled plasma (CCP) sources, electron cyclotron resonance sources and surface wave excited plasma sources, are being extensively investigated [1–4]. Among these plasma sources, ICPs have been acted as a great candidate because of its desirable characteristics, e.g. relatively higher plasma density, low ion damage to the substrate, and the possibility of independent ion energy control by the addition of radio-frequency (RF) bias [5–10]. ICPs also can be classified into planar ICP and cylindrical ICP according to the geometrical shape of reactors and the position of excitation antenna [7, 8]. The planar ICP is commonly used in the semiconductor fabrication, wafer etching and flat-panel display process; whereas the cylindrical ICP has wider application in the fields of RF ion source implantation, space propulsion, and plasma-based surface modification of various material, etc due to its larger discharge volume [2, 8–12]. Irrespective of the planar ICP or cylindrical ICP, both of them face the problem that how to simultaneously produce high-density uniform plasma in radial direction [13, 14].

For planar ICP, in order to obtain high-density uniform plasma, various methods (e.g. changing the antenna shape [5, 6], employing multiple low-inductance antenna units [15], and using dual antenna or dual frequency discharge [16–19]) have been attempted by many researchers. For cylindrical ICP, the main interaction between electromagnetic field and plasma takes place in the skin layer near the plasma boundary [14], thus RF power is non-uniformly deposited in radial direction. The non-uniformity of power deposition directly leads to the occurrence of plasma non-uniformity. This phenomenon will become more severe under the condition of higher input power and higher gas pressure [13]. To solve the problem, researchers had done a lot of work, and numerous articles had been published experimentally in the past decades [20–28]. Bang *et al* [20] designed a dual-frequency ICP

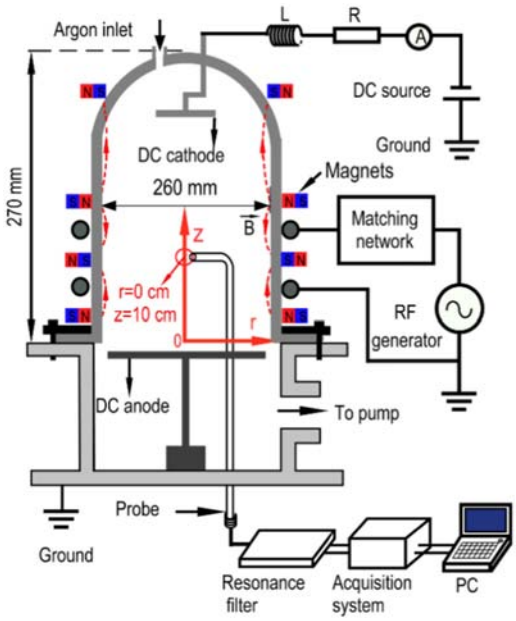

Figure 1. Sketch of the DCE-ICP source.

Figure 2. The electrode structures of (a) DC plate cathode and (b) DC grid anode.

configuration by installing 13.56 MHz and 400 kHz antenna at the center and edge of the chamber, and measured the radial distribution of plasma density. Their experimental result showed that uniform density distribution can be achieved by modulating the power ratio between 13.56 MHz and 400 kHz. Chen *et al* [21] proposed a method based on the nonlinear interaction among the multiple internal antennas to build up a high density uniform plasma. In the experiment of Kim *et al* [22], they installed an additional cylindrical ICP source at the center of the ferrite enhanced ICPs, and found that the uniform plasma density distributions were achieved through a simultaneous discharge of the cylindrical ICP and the ferrite enhanced ICPs (cylindrical ICP + Ferrite ICPs). Besides, Setsuhara and Takenaka *et al* [23, 28] adopted multiple low-inductance antenna units to sustain the discharge in a 500 mm cylindrical plasma source. Other methods about innovation of discharge device in cylindrical ICP can also be found everywhere [24–27].

In this paper, a direct current enhanced inductively-coupled plasma (DCE-ICP) source which consists of a typical cylindrical ICP source and a plate-to-grid DC electrode, is specially designed to obtain high-density uniform plasma over a large scale of 260 mm. The plate-to-grid DC electrode is concentrically placed inside the cylindrical ICP source, and the stable single DC discharge can be achieved. Then the effects of DC discharge on the uniformity and density of cylindrical ICP source are investigated, and the underlying physical mechanism are analyzed. Moreover, the nonlinear enhancement effect of electron density is confirmed by comparing the plasma density produced by single RF and DC + RF hybrid discharge at constant total power.

2. Experimental setup

Figure 1 shows the sketch of the DCE-ICP source which consists of a DC plate-to-grid electrode and a typical cylindrical ICP source. The cylindrical ICP source mainly consists of a stainless steel pedestal and a cylindrical quartz chamber with an inner diameter of 260 mm and a height of 270 mm. The bottom plane center of the quartz chamber is set as $z = 0$ cm, $r = 0$ cm and the positive direction of z axis is straight up. The quartz chamber connects the grounded pedestal with a flange. A two-turn copper coil antenna (axial position: $z = 7$ cm and $z = 13$ cm) winds around the outer surface of the quartz chamber, and then connects with an RF power generator of 13.56 MHz (SKY5000 W) through an L-type matching network. The copper tubes were cooled with water. The reflected power can be controlled by adjusting the matching network and maintained under 1% of discharge power.

The electrode structure of (a) DC cathode and (b) DC anode in the experiment are shown in figure 2. The molybdenum sheet with a diameter of 80 mm and a thickness of 1.5 mm, which has been used as DC cathode, is installed at the top ($z = 210$ mm) of the discharge quartz chamber horizontally. The DC anode with a diameter of 230 mm is a circular grid electrode as shown in figure 2(b), and is made of stainless steel. The anode is located at the bottom of the discharge quartz chamber, and its center is at the position of $z = -10$ mm and $r = 0$ mm. The axial distance between DC cathode and anode is 220 mm. In order to reduce electromagnetic interference to the DC power supply, an inductance L (110 μH) and a resistor R (300 Ω) are connected into the DC circuit. Meanwhile, an ampere meter with 0.1 mA precision is also connected into the circuit to measure the current through DC circuit, and then the DC power can be calculated from the equation $P_{dc} = UI - I^2R$ (U is the DC output voltage, R is fixed resistance and I is the measured current). Moreover, a floating Langmuir double probe made of two cylindrical tungsten wires with a diameter of 0.2 mm and a

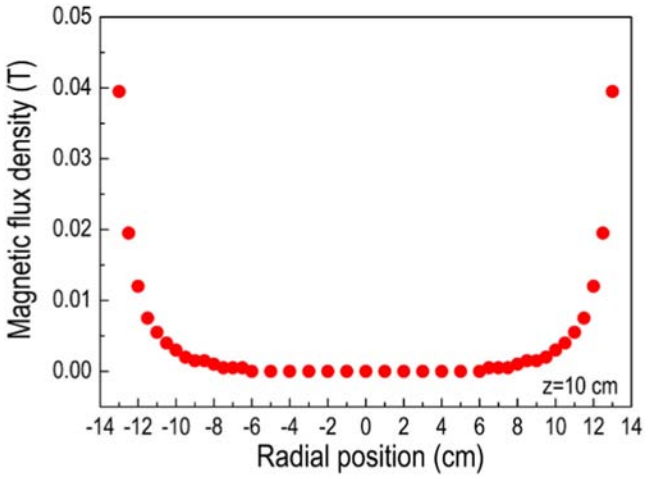

Figure 3. The measured radial distribution of the cusp magnetic field at the plane of $z = 10$ cm.

length of 5 mm is placed at the position of $z = 10$ cm, and is able to move azimuthally to measure electron density and electron temperature. In our experiments, the two-turn high-frequency antenna is installed at the position of $z = 7$ cm and $z = 13$ cm, thus $z = 10$ cm is corresponding to middle part of the radio-frequency coil along the axial position. The maximum value of electron density along axial position presents at the position of $z = 10$ cm. (the axial distribution of electron density is not shown here) Therefore, in this article, we selected the plane of $z = 10$ cm as a typical measurement plane. Besides, in order to avoid the disturbance of RF signal incursion (second harmonics and even high harmonics) on the probe, a resonance filter is equipped between the probe and acquisition system, and the probe is floated to the ground.

In this experiment, the gas is evacuated by a turbo-molecular pump (KYKY F-110/110) backed by a two-stage rotary-vane vacuum pump (KYKY RVP-4), and the typical base pressure of 1.7×10^{-5} Torr can be achieved routinely. A mass-flow controller (D008-1D/ZM) and compound vacuum gauge (ZDF-11A1) are respectively used to regulate the gas inflow rate and measure the discharge pressure. Meanwhile, all the measurements are conducted using argon as working gas. Additionally, in order to reduce the energy loss at the chamber wall due to the ambipolar diffusion [29], four magnetic rings which consists of many small magnets are placed concentrically at the surface of quartz tube to form a cusp magnetic field. The measured radial distribution of the magnetic flux density by Gauss meter (model LZ-643) at $z = 10$ cm are shown in figure 3. The field mainly concentrates in the vicinity of chamber boundary and decreases exponentially from the boundary to the edge, so there is almost no magnetic field in the bulk plasma. Therefore, the measurement accuracy of Langmuir double probe can be ensured.

3. Results and discussion

In this section, the radial density distributions of single RF discharge at different gas pressures are firstly investigated. Then, at a typical pressure of 50 mTorr, we further investigated the plasma properties of single DC discharge, e.g. radial density distribution, electron temperature distribution, and electrical parameters (the DC discharge voltage and current) at different DC powers, then compared them with the corresponding plasma properties of DC + RF hybrid discharge. For DC + RF hybrid discharge, the RF power is fixed at 180 W, and then the DC power varies. Moreover, the nonlinear enhancement effect of plasma density with hybrid discharge is specifically stressed, and the underlying physical mechanism is discussed.

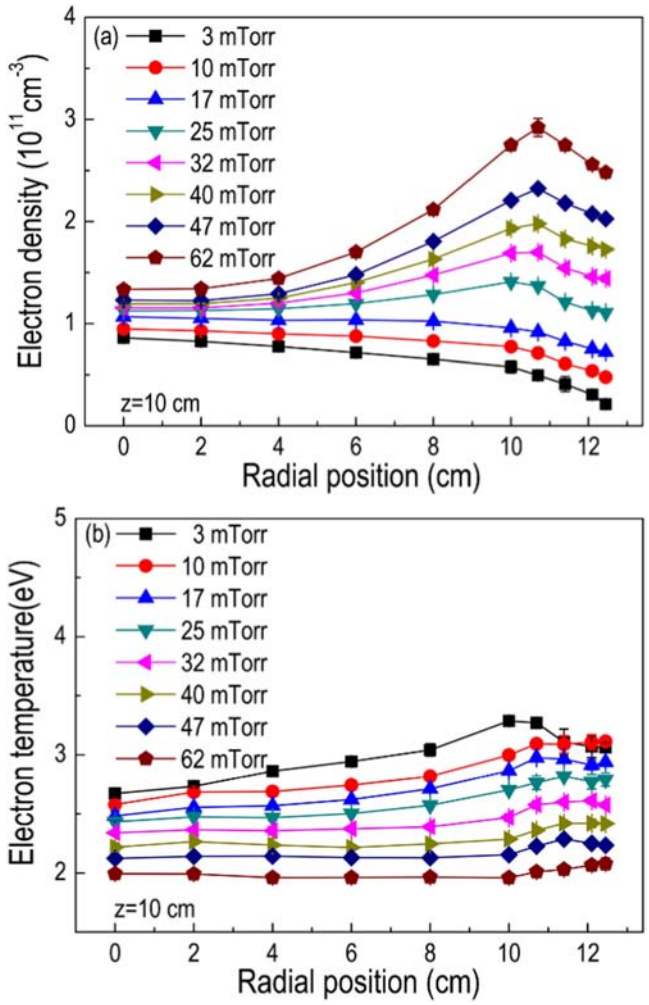

Figure 4. The radial distributions of (a) electron density and (b) electron temperature at RF power 180 W and various gas pressures.

3.1. Single RF discharge

Figure 4 shows the radial distributions of (a) electron density and (b) electron temperature at RF power 180 W and various gas pressures. The measurement plane is at $z = 10$ cm. As seen, the distributions show a 'half convex-like structure' at low gas pressure (3–17 mTorr) and a 'half saddle-like structure' at high pressures (25–62 mTorr). This is maybe related to the transition of electron kinetics from nonlocal to local kinetics. For typical ICP discharge, discharge power is coupled to the plasma through the interaction between electrons

and the vortex electric field. The vortex electric field induced by oscillating RF magnetic field is mainly localized in the vicinity of the antenna coil, as observed by You *et al* [30] and Li *et al* [31]. Thus the electron heating mainly presents in the vicinity of antenna coil. Moreover, at a high pressure where the electron energy relaxation length λ_ε is shorter than the plasma characteristic dimension L, the electron property is local kinetic property [32]. The electrons heated by the vortex electric field near the plasma boundary lose their energy through inelastic collisions (ionization, excitation, etc) in the skin layer before they reach the plasma bulk. [33–35]. Therefore, the inelastic processes are mainly localized at the skin layer. As a result, the RF power is mainly deposited in the skin layer near the chamber boundary, which further leads to the occurrence of half saddle-like structure, as shown in figure 4(a).

On the contrary, at the low pressure where $\lambda_\varepsilon > L$, the electrons can gain net energy from the vortex electric field and transverse the skin layer in a short time, and then wander around in the entire volume before their energy is exhausted [32, 35]. Therefore, the maximum ionization region is no longer localized in the skin layer and it is not identical to the region that maximum electric field exists. Moreover, the plasma potential is maximal at the chamber center due to ambipolar diffusion. In this case, electrons experience the ambipolar potential as the negative potential to be overcome, while the ions are accelerated from the center toward the boundary. Thus, the electrons obtain maximal kinetic energy at the discharge center where the maximum plasma potential is presented [36]. As a result, the maximum ionization region occurs near the chamber center where the RF field is absent or weak, which is also the typical characteristic of nonlocal electron kinetics [35]. The observed half convex-like shape of electron density is consistent with the experimental results in low pressure planar ICP [36, 37] and the simulation results in cylindrical ICP using a self-consistent one-dimensional model [30].

The radial distributions of electron temperature at RF power 180 W and different gas pressures are given in figure 4(b). From the figure it can be clearly seen that the electron temperature decreases continuously as gas pressure increases. This can be understood by the fact that particles number density is proportional to gas pressure [35, 38]. When the particles number density is high, the collision probability among the electrons and the neutrals is so high that the electrons frequently collide with other particles and lose their energy, further, lead to the decrease of electron temperature. Moreover, the electron temperature decrease with the increase of gas pressure is also a characteristic feature for ICP discharge [38, 39]. In addition, the higher electron temperature occurs at the chamber boundary is related to the heating in vortex electric field. The electric field is mainly located at the chamber boundary, which have been proved by Li *et al* [31] by using finite difference method in cylindrical ICP.

As analyzed above, the electron density shows different distributions at different gas pressures. However, in this experiment, we focus on the effect of DC discharge on RF discharge, therefore, a typical gas pressure of 50 mTorr is fixed to investigate the plasma characteristics of DCE-ICP source in the following experiments.

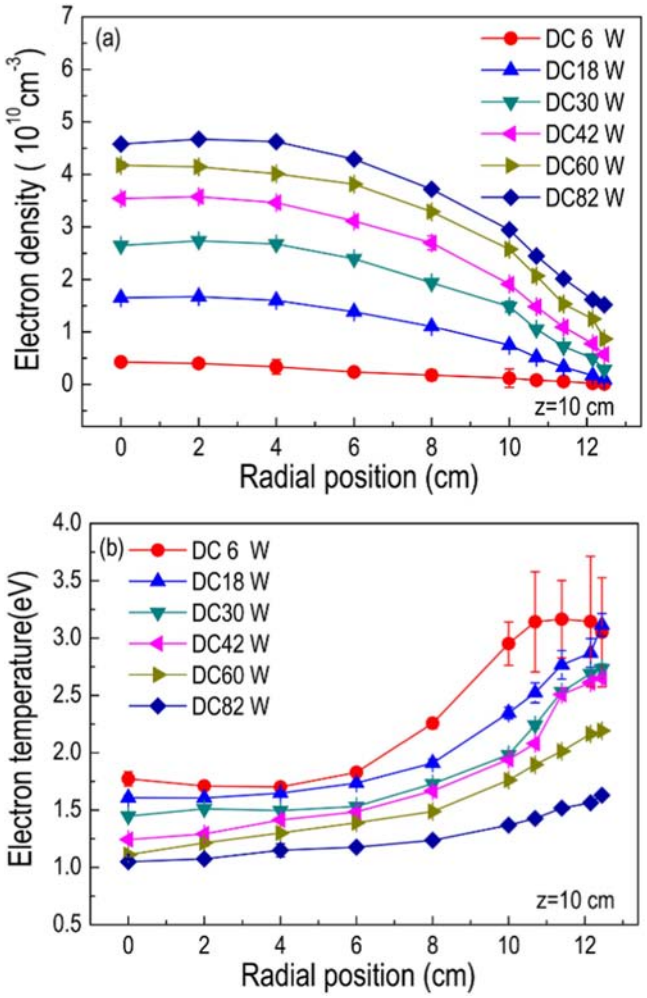

Figure 5. Dependence of (a) electron density and (b) electron temperature on radial position for single DC discharge at 50 mTorr argon pressure and different DC powers.

3.2. Single DC discharge

Figure 5 shows the radial distributions of (a) electron density and (b) electron temperature for single DC discharge at gas pressure of 50 mTorr and different DC powers 6, 18, 30, 42, 60 and 82 W. The measurement is conducted at the plane of $z = 10$ cm. Each data point is measured at least three times, and error bars are given by calculating the standard deviation of the data. As shown in figure 5(a), the electron density decreases from the chamber center to chamber boundary regardless of the DC power. This is mainly due to the transport and diffusion of charged particles along the radial position [35]. For DC discharge of the plane-parallel electrode, the radial transport and diffusion of charged particles can be determined by solving the free or ambipolar diffusion equation [35]. And the complete solution of the equation is a parabola, which is in accord with the evolution tendency of electron density in our experiment.

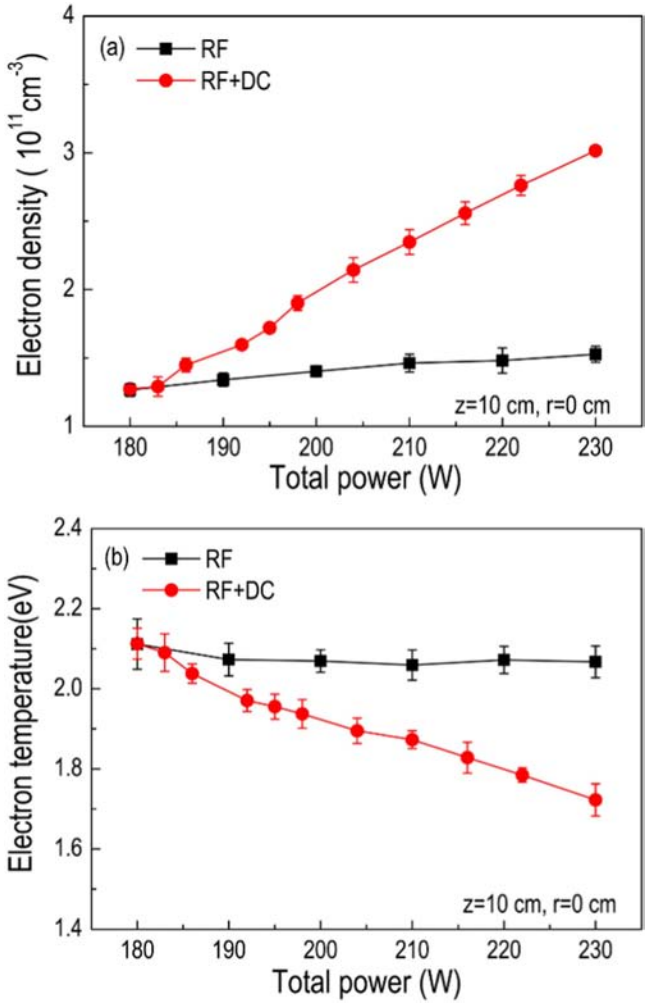

Figure 6. Comparisons of (a) electron density and (b) electron temperature between single RF discharge and DC + RF hybrid discharge at the same total power with 50 mTorr Ar.

The radial distributions of electron temperature at different DC powers are given in figure 5(b). As seen, the distributions show the tendencies that the higher electron temperature centralizes on the chamber boundary due to the main ionization region presents at chamber center. Moreover, with the increase of DC power from 6 to 82 W, the electron temperature decreases gradually. This result may be explained as follows: as DC power increases, the electron density increases as shown in figure 5(a), which will lead to more frequent electron–electron collision because electron–electron collision frequency is proportional to electron density [14]. In addition, a two-step ionization may become enhanced, which leads to the reduction of electron temperature with increasing electron density [14, 18].

3.3. DC + RF hybrid discharge

Figure 6 shows the comparisons of (a) electron density and (b) electron temperature between single RF discharge and DC + RF hybrid discharge at the same total power. As shown in figure 6(a), when the discharge is sustained by single RF discharge, the electron density increases slightly from $1.45 \times 10^{11}\,\mathrm{cm}^{-3}$ to $1.745 \times 10^{11}\,\mathrm{cm}^{-3}$ as RF power increases from 180 to 230 W. However, when the discharge is sustained by DC + RF hybrid discharge that fixes RF power at 180 W and increases the DC power from 0 to 50 W, the electron density increases dramatically from $1.45 \times 10^{11}\,\mathrm{cm}^{-3}$ to $3.44 \times 10^{11}\,\mathrm{cm}^{-3}$. Notably, the electron density of DC + RF hybrid discharge is obviously higher than that of single RF discharge when the total power remains in the same value. This phenomenon can be attributed to the nonlinear enhancement effect between DC discharge and RF discharge. The similar nonlinear enhancement effect has been proved by Chen *et al* [21, 40] with discharge of multiple cylindrical ICP sources.

For DC + RF hybrid discharge, when the molybdenum sheet is applied to negative voltage, the ions produced by RF discharge are accelerated to bombard the molybdenum cathode, and, accordingly, abundant secondary electrons are generated [41]. The secondary electrons are then accelerated in the electric fields of cathode sheath, and collide with the neutral particles, therefore more electron–ion pairs are generated by the collision ionization process [35]. Moreover, because the plasma potential of chamber center which generated by RF discharge is positive due to ambipolar diffusion [14, 42], the axial electric field is formed between cathode sheath and bulk plasma. Under the effect of the axial electric field, the electrons produced by DC discharge moves to the center of the discharge chamber, and they also lose energy to the bulk plasma by collisions against the background particles. As a result, more electrons are generated and poured into the bulk plasma, and some of them are captured and reutilized efficiently by RF discharge, consequently, the electron density is improved dramatically. This means an auxiliary DC discharge at chamber center will give rise to a lot of ionization and the nonlinear enhancement of electron density in the bulk. This process may be similar to the seed electron effect of atmosphere atmospheric discharge [43] and the density enhancement effect in DC superposed CCP discharge [44–48]. Kawamura *et al* [41, 49] and Zhang *et al* [47] reported simulation results of DC superposed CCP discharge, and found that DC discharge can significantly improve electron density, which is consistent with the experimental phenomenon of our experiment.

The comparison of electron temperature between single RF and DC + RF hybrid discharge versus the total input power are given in figure 6(b). As shown in figure 6(b), the electron temperature basically remains in an unchanged value about 2.11 eV in the operation of single RF discharge, while it decreases monotonically from the value of 2.11–1.72 eV in the operation of DC + RF hybrid discharge. The decreasing trend of electron temperature is desirable for electronic devices which required plasma processing during the device processing because lower electron temperature means low damage to the substrate [50, 51]. The obvious decrease of electron temperature for DC + RF hybrid discharge can be explained as follows: as DC power increases, the amplitude of negative voltage applied to the molybdenum sheet becomes larger as shown in figure 7, which leads to the stronger axial electric field between DC cathode and bulk plasma. With the

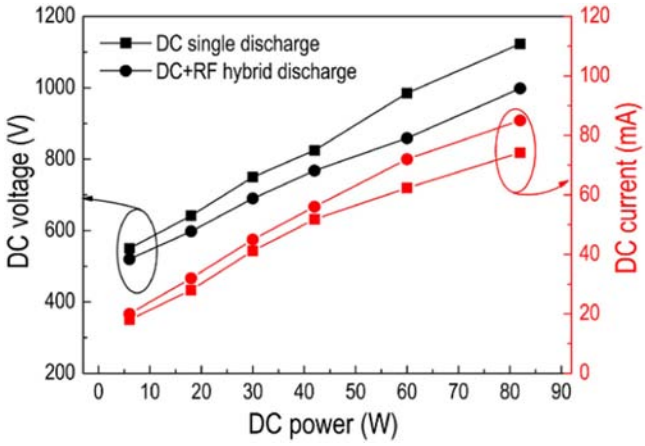

Figure 7. The DC voltage and current as a function of DC power in the case of single DC and DC + RF hybrid discharge with 50 mTorr Ar.

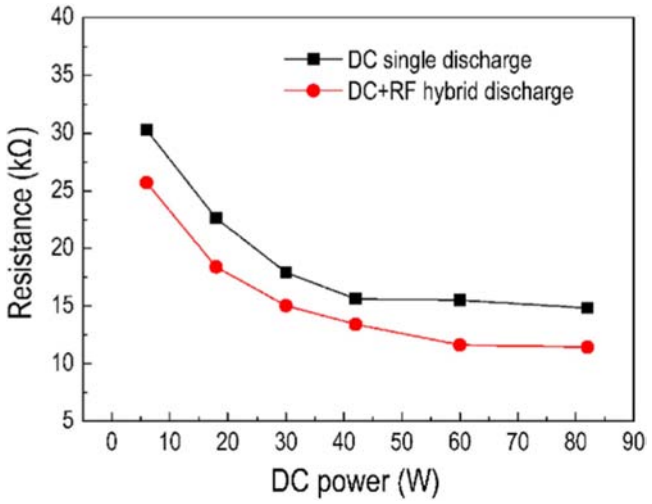

Figure 8. The calculated values of plasma resistance as a function of DC power in the case of single DC and DC + RF hybrid discharge with 50 mTorr Ar.

effect of axial electric field, more ions produced by RF discharge bombard the DC cathode to generate more seed electrons. The seed electrons pour into the bulk plasma and frequently collide with other particles, including electron–electron collision and electron–neutral collision, which leads to the reduction of the electron temperature.

DC discharge voltage and current are also important because the increase of electron density with DC + RF hybrid discharge is related to the secondary electrons produced by ion bombardment of Mo electrode, whereas the bombardment effect is directly related to the DC voltage. Therefore, the variation of DC discharge voltage and current with DC power in the case of single DC discharge and DC + RF hybrid discharge are shown in figure 7. It can be seen from figure 7, both the DC voltage and current increase linearly with DC power, regardless of single DC or DC + RF hybrid discharge. The voltage increases from 550 to 1123 V accompanied by an increase in current from 18 to 74.2 mA for single DC discharge, while the voltage increases from 520 to 998 V accompanied by an increase in current from 20.1 to 84.8 mA for DC + RF hybrid discharge. Moreover, it can be found that the voltage of DC + RF hybrid discharge is lower than that of single DC discharge by comparing the voltage between single DC and DC + RF hybrid discharge at same DC output power. This result is due to different plasma resistance between single DC and DC + RF hybrid discharge. In the case of DC + RF hybrid discharge, the discharge has been ignited by RF discharge before applying DC voltage additionally, thus plasma resistance of hybrid discharge is relative lower than that of single DC discharge.

In order to compare the plasma resistance between single DC and DC + RF hybrid discharge roughly, the calculated values of plasma resistance as a function of DC power are given in figure 8 according to the equation $R = U/I - 300$ (the corresponding value of U and I can be found in figure 7). It can be seen from figure 8, plasma resistance decreases gradually with DC power, i.e., from 30.26 to 14.83 kΩ for single DC discharge, while from 25.7 to 11.44 kΩ for DC + RF hybrid discharge. It indicates that the relative low plasma resistance of DC + RF hybrid discharge at the same DC power.

To further investigate the effect of DC discharge on the spatial distribution of plasma parameter, figure 9 presents the radial distribution profiles of (a) electron density and (b) electron temperature at fixed RF power 180 W and different DC powers 0 W, 6 W, 18 W, 30 W, 42 W, 60 W and 82 W, respectively. It can be seen from figure 9(a) that the density radial distribution shows a 'half saddle-like structure' due to nonlocal electron kinetics in the operation of single RF discharge 180 W. However, the distribution evolves from a 'half saddle-like structure' to a 'half convex-like structure' as the DC power increases from 0 to 82 W, which indicates that the plasma uniformity can be modulated in the operation of DC + RF hybrid discharge.

The improvement of plasma uniformity can be explained by the different enhancement effect of DC discharge on electron density at the chamber center and chamber boundary. When the discharge is sustained by DC + RF hybrid discharge, the majority of electrons produced by DC discharge pour into the chamber center, and collide with other particles to lead to a nonlinear increase in electron density, as explained in figure 6(a). Moreover, the electrons also lose their energy to the bulk plasma by collisions against the background particles, and become low-energy electrons during this process. The injection of low-energy electrons will lead to the decrease of plasma potential at chamber center. As a result, a radial electric field is formed from the chamber wall to chamber center due to the decrease in plasma potential at chamber center. Under the effect of radial electric field, the electrons at chamber center will move toward the wall and collide with the skin layer, thus leads to the increase of electron density and decrease of plasma potential at chamber boundary until establishing a new equilibrium state. Furthermore, the radial distribution shows good uniformity when the DC power is adjusted to 60 W as shown in figure 9(a).

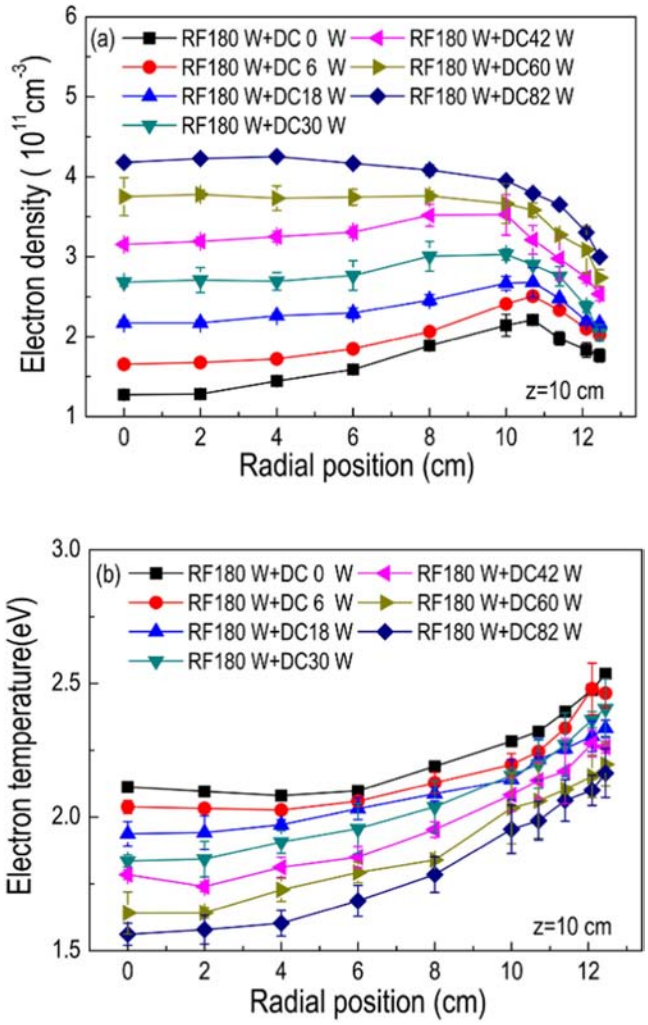

Figure 9. Radial distributions of (a) electron density and (b) electron temperature at fixed RF power 180 W and different DC powers with 50 mTorr Ar.

Thus it is deduced that there exists synergistic discharge between DC and RF discharge, and the radial distributions of electron density in this region are controlled by DC and RF discharge synergistically.

As shown in figure 9(b), the radial distribution of electron temperature shows the tendency that higher electron temperature is located at the chamber boundary in the operation of single RF discharge, which is due to the presence of induced vortex electric field at chamber boundary [30]. The electrons near the boundary can obtain the energy from the electric field and diffuse to the inside of the chamber and collide with other particles, then lose their energy. Therefore, the electron temperature at the chamber boundary is higher than that at chamber center. Lee *et al* [52] have experimentally shown that electron can be heated by inductive field in inductively coupled plasma system. Moreover, the electron temperature decreases successively as the DC power increases from 0 to 82 W, and the decreasing rate of electron temperature at the center is faster than that at chamber boundary. This is mainly caused by the fact that DC discharge has more obvious effect on the ionization efficiency of plasma located

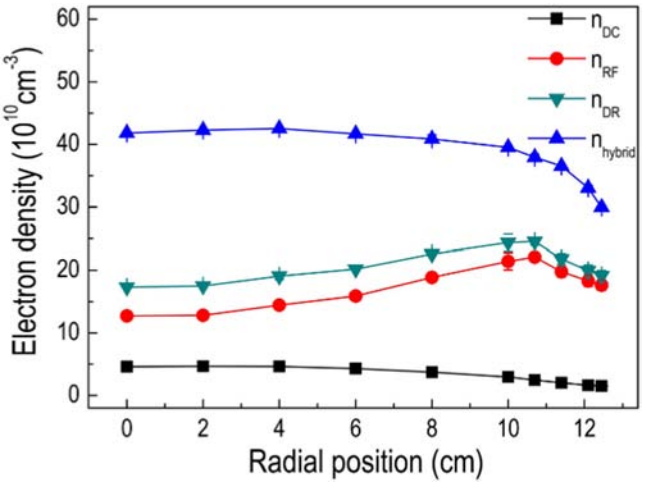

Figure 10. The radial distributions of n_{DC}, n_{RF}, n_{DR} and n_{hybrid}, where n_{DC}, n_{RF} and n_{hybrid} are the electron density of single DC discharge (82 W), single RF discharge and DC + RF hybrid discharge with 50 mTorr Ar. n_{DR} is the linear summation of n_{DC} and n_{RF}.

at chamber center due to the limited area of DC cathode. As explained in figure 9(a), the majority of electrons produced by DC discharge mainly pours into the center of chamber, thus the frequent electron–neutral collision and electron–electron collision occurs at the chamber center, which leads to the obvious decrease of electron temperature at the chamber center, as displayed in figure 9(b).

3.4. Nonlinear enhancement effect

In order to further investigate the nonlinear enhancement phenomenon of plasma density under the condition of DC + RF hybrid discharge, figure 10 presents the radial distributions of n_{DC}, n_{RF}, n_{DR} and n_{hybrid}, where n_{DC}, n_{RF} and n_{hybrid} are the electron density of single DC discharge (82 W), single RF discharge and DC + RF hybrid discharge. n_{DR} is the linear summation of n_{DC} and n_{RF}. As shown in figure 10, it can be seen that the radial distribution of n_{hybrid} is not only dramatically larger than that of n_{DC} and n_{RF}, but also larger than that of n_{DR}, especially in the center of the chamber. This indicates that a special mechanism of plasma density enhancement exists when DC and RF sustain the discharge, simultaneously.

Moreover, for scaling the nonlinear enhancement phenomena, the nonlinear enhancement factor β is defined as $\beta = n_{hybrid}/n_{DR}$. The ratio β mainly reflects the effect of DC discharge on RF discharge, and the value of it could be $\beta < 1$, $\beta = 1$, or $\beta > 1$, corresponding to that electron density is reduced nonlinearly, added linearly, or enhanced nonlinearly, respectively. The calculated value of β varying with the radial position at fixed RF 180 W and different DC powers are shown in figure 11. As shown, in all range of radial position, β is no less than 1 which indicates the electron density is enhanced nonlinearly at the whole radial space. Whereas the maximum value of β nearly presents at the center of the chamber and decreases from the chamber center to boundary gradually regardless of the value of DC power, which means that the nonlinear enhancement effect of

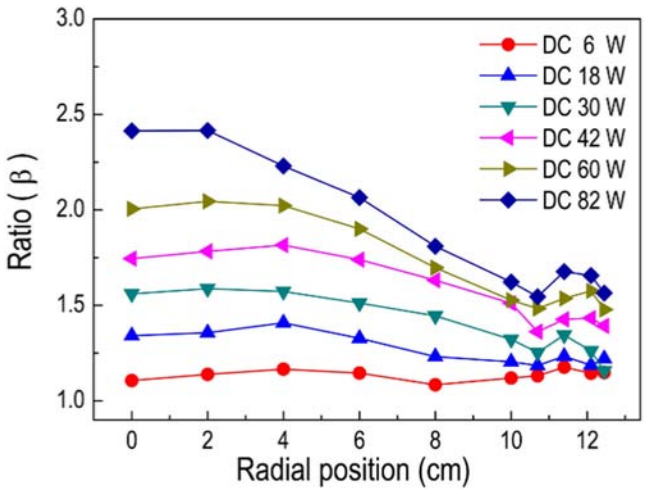

Figure 11. The radial distribution of β at the fixed RF power 180 W and various DC powers with 50 mTorr Ar.

electron density is the most conspicuous at the chamber center in the case of DC + RF hybrid discharge. This is because the DC discharge region is mainly concentrated in the underneath of the DC cathode, as explained in figure 5(a).

4. Conclusions

In this work, we designed a DCE-ICP hybrid discharge source by installing a DC plate-to-grid electrode inside the cylindrical ICP chamber, and investigated the plasma characteristics of single RF discharge and DC + RF hybrid discharge experimentally. It is found that the DC + RF hybrid discharge shows higher electron density than single RF discharge at the same total input power due to the nonlinear enhancement effect. Moreover, a better uniform plasma can be obtained with the operation of DC + RF hybrid discharge owing to the obvious enhancement of electron density at the chamber center, and the radial distribution of electron density can be modulated by DC power. Furthermore, the utilization of DC power decreases the electron temperature effectively, which is mainly attributed to higher ionization efficiency for DC + RF hybrid discharge. Indeed, our study provides some insights into how to obtain high-density uniform plasma along radial direction in cylindrical ICP.

Acknowledgments

This work is supported by National Natural Science Foundation of China (Grant No. 11475038.)

References

[1] Hong S P *et al* 2010 *Japan. J. Appl. Phys.* **49** 080217
[2] Tarey R D *et al* 2016 *Plasma Sources Sci. Technol.* **26** 015009
[3] Mikami H *et al* 2005 *Japan. J. Appl. Phys.* **44** 3817
[4] Liu Y X *et al* 2017 *Phys. Plasmas* **24** 073512
[5] Li L S *et al* 2008 *Chin. Phys. Lett.* **25** 2144
[6] Leou K C *et al* 1999 *Japan. J. Appl. Phys.* **38** 4268
[7] Lee H C, Lee M H and Chung C W 2010 *Appl. Phys. Lett.* **96** 071501
[8] Speth E *et al* 1999 *Fusion Eng. Des.* **46** 383
[9] Charles C, Boswell R W and Takahashi K 2012 *Plasma Phys. Control. Fusion* **54** 124021
[10] Nabhiraj P Y *et al* 2010 *Nucl. Instrum. Methods Phys. Res.* A **621** 57
[11] Charles C and Boswell R W 2012 *Plasma Sources Sci. Technol.* **21** 022002
[12] Cheng Y *et al* 2015 *Chin. Phys. Lett.* **32** 058102
[13] Wang Z *et al* 2015 *Plasma Sci. Technol.* **17** 191
[14] Godyak V A, Piejak R B and Alexandrovich B M 2002 *Plasma Sources Sci. Technol.* **11** 525
[15] Jung S J, Kim K N and Yeom G Y 2006 *Thin Solid Films* **506-507** 460
[16] Mishra A and Yeom G Y 2013 *Surf. Coat. Technol.* **237** 440
[17] Kim K N *et al* 2006 *Appl. Phys. Lett.* **89** 251501
[18] Kim T H *et al* 2013 *Japan. J. Appl. Phys.* **52** 05EA02
[19] Mishra A *et al* 2012 *Plasma Sources Sci. Technol.* **21** 035018
[20] Bang J Y *et al* 2011 *Phys. Plasmas* **18** 073507
[21] Chen Z P *et al* 2010 *Phys. Plasmas* **17** 103503
[22] Kim H J *et al* 2015 *J. Appl. Phys.* **117** 153302
[23] Setsuhara Y, Tsukiyama D and Takenaka K 2008 *Surf. Coat. Technol.* **202** 5238
[24] Lee J, Kim K H and Chung C W 2017 *Phys. Plasmas* **24** 023503
[25] Lee K *et al* 2008 *Plasma Sources Sci. Technol.* **17** 015014
[26] Liu L *et al* 2015 *J. Appl. Phys.* **118** 083303
[27] Uhm S *et al* 2004 *Phys. Plasmas* **11** 4830
[28] Takenaka K *et al* 2006 *Japan. J. Appl. Phys.* **45** 8046
[29] Kim K N, Kim M S and Yeom G Y 2006 *Appl. Phys. Lett.* **88** 161503
[30] You K I, Yoon N S and Hwang S M 1999 *Surf. Coat. Technol.* **114** 60
[31] Li W P *et al* 2008 *J. Appl. Phys.* **104** 083306
[32] Cunge G *et al* 2001 *J. Appl. Phys.* **89** 3580
[33] Godyak V A and Piejak R B 1993 *Appl. Phys. Lett.* **63** 3137
[34] Seo S H *et al* 2000 *Phys. Rev.* E **62** 7155
[35] Lieberman M A and Lichtenberg A J 2004 *Principles of Plasma Discharges and Materials Processing* 2nd edn (New York: Wiley)
[36] Lee H C and Chung C W 2013 *Phys. Plasmas* **20** 101607
[37] Lee H C and Chung C W 2015 *Phys. Plasmas* **22** 053505
[38] Lee D S, Lee Y K and Chang H Y 2004 *Plasma Sources Sci. Technol.* **13** 701
[39] Godyak V A and Alexandrovich B M 2004 *Phys. Plasmas* **11** 3553
[40] Chen Z P *et al* 2011 *Plasma Sci. Technol.* **13** 175
[41] Kawamura E *et al* 2008 *Plasma Sources Sci. Technol.* **17** 045002
[42] Zhou L F *et al* 2015 *Vacuum* **119** 209
[43] Gherardi N *et al* 2000 *Plasma Sources Sci. Technol.* **9** 340
[44] Wang M M and Kushner M J 2010 *J. Appl. Phys.* **107** 023308
[45] Wang M M and Kushner M J 2010 *J. Appl. Phys.* **107** 023309
[46] Diomede P *et al* 2012 *J. Phys. D: Appl. Phys.* **45** 175204
[47] Zhang Q Z, Wang Y N and Bogaerts A 2014 *J. Appl. Phys.* **115** 223302
[48] Yamaguchi T *et al* 2012 *J. Phys. D: Appl. Phys.* **45** 025203
[49] Kawamura E *et al* 2007 *J. Vac. Sci. Technol.* A **25** 1456
[50] Kato K *et al* 2000 *Appl. Phys. Lett.* **76** 547
[51] Phukan A, Mishra M K and Chakraborty M 2007 *J. Phys. D: Appl. Phys.* **40** 3616
[52] Lee H C, Lee M H and Chung C W 2010 *Appl. Phys. Lett.* **96** 041503